Volume 1 | Number 1 | Jan 2013 | Pages 1–100

Catalysis
Science &
Technology

www.rsc.org/catalysis

ROYAL SOCIETY
OF CHEMISTRY

Journal Name

ARTICLE

Hydrothermal synthesis of octahedra-based layered niobium oxide and its catalytic activity as a solid acid

Toru Murayama, Junli Chen, Jun Hirata, Keeko Matsumoto and Wataru Ueda,

Layered-structure type niobium oxides were synthesized by the hydrothermal method by using ammonium niobium oxalate as a precursor. The synthesized niobium oxide showed characteristic peaks at $2\theta = 22.7°$ and $46.2°$ in an X-ray diffraction pattern (Cu-Kα), indicating linear corner-sharing of NbO_6 octahedra in the c-direction. From Raman measurement, the layered-structure type niobium oxide was composed of NbO_6 octahedra and $\{Nb_6O_{21}\}$ pentagonal units. The presence of micropores was confirmed by N_2 adsorption at low pressure (1.0×10^{-6}), indicating that the arrangement of the a-b plane was an interconnection of crystal structure motifs of $\{Nb_6O_{21}\}$ units and micropore channels but without long-range order (deformed orthorhombic). Ammonium cation and water were desorbed from the deformed orthorhombic niobium oxide by calcination at 400 ˚C, and Brönsted acid sites were formed. The deformed orthorhombic niobium oxide showed high catalytic activity as a solid acid compared to the catalytic activities of other crystalline niobium oxides. The order of catalytic activity for the alkylation of benzyl alcohol and anisole was: deformed orthorhombic $Nb_2O_5 >$ TT-Nb_2O_5, amorphous $Nb_2O_5 >>$ T-Nb_2O_5, pyrochlore Nb_2O_5.

Introduction

Niobium oxide is widely used in catalysis and in electrochromic and photoelectrochemical devices.[1, 2] Niobium oxide (or hydrated niobium oxide) has been used especially as a water-tolerant solid acid catalyst for many reactions such as alkylation, esterification, hydrolysis, dehydration and hydration.[3, 4] Hydrated niobium oxide ($Nb_2O_5 \cdot nH_2O$, niobic acid) has a high acid strength ($H_0 \leq -5.6$) and possesses Lewis and Brönsted acidity. Therefore, much effort has been focused on the preparation of new morphologies of nanocrystalline niobium oxide (or hydrated niobium oxide) in order to obtain the niobium oxide with a high surface area, such as nanoparticles,[5, 6] rods,[7, 8] wires,[9] and nanoplates.[10–12] Niobium oxide forms different polyhedra structures and transforms its phase depending on heat treatment. Amorphous niobium oxide, $Nb_2O_5 \cdot nH_2O$, possesses distorted NbO_6 octahedra, NbO_7 pentagonal bipyramids and NbO_8 hexagonal bipyramids as structural units.[13, 14] With heat treatment of $Nb_2O_5 \cdot nH_2O$, pseudohexagonal niobium oxide (TT-Nb_2O_5) is formed at 300-500 ˚C, orthorhombic niobium oxide (T-Nb_2O_5) at 700- 800 ˚C and monoclinic niobium oxide (H-Nb_2O_5) is formed at temperatures higher than 1000 ˚C. With increases in the heat treatment temperature and the degree of crystallinity, catalytic activity as a solid acid (Brönsted acidity) and surface area are decreased.[15] Therefore, not the protons formed on ordered crystalline structure but the protons formed on distorted polyhedra in amorphous $Nb_2O_5 \cdot nH_2O$ have been regarded as active sites as Brönsted acid.

For improving the Brönsted acidity and catalytic properties of niobium oxide, modification of niobium oxide or supported niobium oxide with sulfate and phosphate has been tried.[16–18] Complex metal oxide such as layered HNbMOx (M = Ti, Mo, W) has been reported as a strong solid catalyst, and M(OH)Nb was regarded to represent a strong Brönsted acid site.[19, 20] Some researchers reported that the acid centers were due to isomorphous substitutions of Nb^{5+} by the higher-valence cation M^{6+} (Mo, W) in the mixed oxide.[21, 22]

We have long studied the relationship between the crystalline structure of complex metal oxides and their catalytic activity.[23–25] Studies on crystalline metal oxides of Mo_3VO_x have demonstrated that the oxidation activities depend on their crystalline arrangement of the pentagonal $\{Mo_6O_{21}\}$ units and MO_6 octahedra in the a–b plane. These materials contain heptagonal channels in their structure. For the synthesis of these catalysts, the formation of a pentagonal $\{Mo_6O_{21}\}$ unit in the precursor solution was important, and the pentagonal unit assembled further into a complex metal oxide under hydrothermal conditions.[26, 27] A complex metal oxide that possess a similar layered-structure in the c-direction by corner-sharing of MO_6 (M= Mo, W, V, Ta, Nb) octahedra has been synthesized by a hydrothermal method.[28–30] These catalysts were found to function as solid acids, the property of which was understood from the structural point of view.

We report herein the synthesis of niobium oxide by a hydrothermal process from niobic acid and niobium oxalates precursors. The Nb atom has a pentagonal bipyramidal environment in the crystal structure of $NH_4[NbO(C_2O_4)_2(H_2O)_2]\cdot nH_2O$,[31] and under hydrothermal conditions, pentagonal $\{Nb_6O_{21}\}$ units may be formed by the hydrolysis of $[NbO(C_2O_4)_2(H_2O)_2]^-$ [32] and then be self-assembled into niobium oxide. The structure and catalytic activity of the obtained niobium oxides were investigated. Various crystalline niobium oxides including pseudohexagonal (TT phase), orthorhombic (T phase), pyrochlore, and amorphous niobium oxide were also prepared, enabling us to discuss the relationships between the crystalline structure and their catalytic activity and acidity.

Experimental

Preparation of niobium oxides

Layered-structure type niobium oxides were synthesized by a hydrothermal method from ammonium niobium oxalate $(NH_4[NbO(C_2O_4)_2(H_2O)_2]\cdot nH_2O)$, denoted as NbO-ANO. Typically, ammonium niobium oxalate (supplied from CBMM) containing 6 mmol Nb was dissolved in 40 mL of deionized water and then sealed in a 60 mL Teflon liner stainless-steel autoclave. Hydrothermal reaction was carried out at 175°C for 3 days. The obtained solid was filtered, washed thoroughly with deionized water, and dried at 80 °C overnight. The same type of niobium oxide was obtained from ammonium niobium oxalate (Aldrich), and similar characterization results were obtained (Table S1). Pseudohexagonal niobium oxide and pyrochlore niobium oxide were also synthesized by a hydrothermal method using a niobic acid $(Nb_2O_5\cdot nH_2O$, Soekawa Chemicals) precursor, denoted as NbO-NA(d) and NbO-NA(c), respectively. 4 mmol based on Nb of niobic acid dispersed in 40 mL deionized water for NbO-NA(c) and 0.25 mmol for NbO-NA(d). The hydrothermal conditions and the following process were the same as these for NbO-ANO. The yields of niobium oxides calculated as Nb_2O_5 were more than 90% for all of the catalysts. The samples were calcined at 400 ^{o}C for 4 h under air before using as catalysts. The rate of temperature increase was 10 ^{o}C min^{-1} from room temperature. For comparison, amorphous niobium oxide was prepared by calcination of niobic acid at 400 ^{o}C for 4 h under air (denoted as NbO-cal).

As-synthesized material (NbO-ANO, 0.3 g) was dispersed in 15 mL of KNO_3 solution (0.1 mol L^{-1}) for ion-exchange treatment. The dispersed sample was stirred at 80 ^{o}C for 8 h. The resulting solid was collected by filtration. Then the sample was washed with water (3 × 100 mL) and dried at 80 ^{o}C overnight. The obtained sample was denoted as NbO-ANO (K$^+$). A NbO-ANO (K$^+$) sample treated with NH_4NO_3 solution was denoted as NbO-ANO (NH$_4^+$). NbO-ANO (NH$_4^+$) was prepared by ion-exchange treatment of NbO-ANO (K$^+$) in 15 ml of NH_4NO_3 solution (0.1 mol L^{-1}) at 80 ^{o}C for 8 h.

Alkylation reaction

A 50 mL round-bottom three-neck flask equipped with a reflux condenser was used as a stirred bed reactor to test the catalytic activities. Typically, a mixture of benzyl alcohol (1 mmol), anisole (50 mmol), and an internal standard, decane (0.5 mmol), was added to the reactor and reaction temperature was adjusted to 100 ^{o}C. Then 0.1 g of a catalyst and a Teflon-coated magnetic stir bar were loaded into the reactor. Aliquots (each 0.1 mL) were collected at intervals. The concentrations of the reactant and product were measured by gas chromatography using a flame ionization detector (GL science GC390B) with a ZB-1 column.

Characterization

The catalysts were characterized by the following techniques. Powder XRD patterns were measured with a diffractometer (RINT Ultima+, Rigaku) using Cu-Kα radiation (tube voltage: 40 kV, tube current: 20 mA). Diffractions were recorded in the range of 4–60° with 5° min^{-1}. Morphology was investigated by using a scanning transmission electron microscope (HD-2000, Hitachi) at 200 kV and 30 μA and a transmission electron microscope (JEM-2100F, JEOL) at 200 kV. The samples were dispersed in ethanol with ultrasonic treatment for several minutes, and drops of the suspension were placed on a copper grid for STEM and TEM observations. Raman spectra were obtained using a spectrometer (in Via Reflex, Renishaw, 2 cm^{-1} spectral resolution) under the conditions of wavelength of 532 nm and collection time of 10 s. N_2 adsorption isotherms at liquid N_2 temperature were measured by using an auto adsorption system (BELSORP MAX, BEL JAPAN) for the samples. The samples before the reactions were heat-treated in air at 400 °C for 2 h (300 °C for the NbO-NA(c) sample). Prior to N_2 adsorption, the catalysts were evacuated under vacuum at 300 °C for 2 h. External surface area was calculated by a multipoint Braunauer-Emmett-Teller (BET) method and the t method. Temperature-programmed desorption (TPD) of ammonia, NH_3-TPD, was employed to measure oxide surface acidity. The experiment was carried out using an auto chemisorption system (BEL JAPAN). The experimental procedure was as follows. The catalyst (ca. 50 mg) was set between two layers of quartz wool and pre-heated under helium (50 mL min^{-1}) at 400 ^{o}C for 1 h (300 ^{o}C for the NbO-NA(c) sample). Then ammonia was introduced at 150 ^{o}C for 30 min. The desorption profile from 150 to 700 ^{o}C was recorded with a mass spectrometer under helium flow (50 mL min^{-1}). Temperature-programmed decomposition mass spectrometry (TPD-MS) measurements were performed from 40 to 700 ^{o}C at a heating rate of 10 ^{o}C min^{-1} in helium flow (50 mL min^{-1}). The decomposed gas molecules were monitored by a mass spectrometer (ANELVA, Quadrupole Mass Spectrometer, M-100QA, BEL Japan), collecting several mass fragments: CO_2 (44), O_2 (32), CO and N_2 (28), H_2O (18, 17, 16) and NH_3 (17, 16, 15). XPS (JPC-9010MC, JEOL) with non-monochromatic Mg-Kα radiation was used for measuring binding energy values of Nb. Binding energy was referred by Au 4f7/2 (84.0 eV) deposited by an auto fine coater (JFC- 1600, JEOL). Measurements of thermogravimetric-differential thermal analysis (TG-DTA) were performed on a TG-8120 (Rigaku) thermogravimetric analyzer. Dry air provided by a pressure tank with a flow rate of 30 mL min^{-1} was used as the carrier gas. The

catalyst sample and a standard were loaded into two alumina pans and heated at 10 °C min⁻¹ to the desired temperature.

Results and discussion

Several niobium precursors were used for hydrothermal synthesis of niobium oxides, and the results of characterization results of the obtained niobium oxides are summarized in Table 1. Fig.1 shows XRD patterns of the obtained niobium oxide samples. When 0.15 mol L⁻¹ of ammonium niobium oxalate ($NH_4[NbO(C_2O_4)_2(H_2O)_2] \cdot nH_2O$) dissolved in 40 mL of water was used as a precursor solution (NbO-ANO), the XRD pattern of NbO-ANO calcined at 400 °C showed only a tense and sharp peak at $2\theta = 22.7°$ and a relatively weak peak at $2\theta = 46.2°$. The peaks at $2\theta = 22.7°$ and 46.2° can be attributed to (001) and (002) planes, respectively. The XRD pattern of NbO-ANO was very similar to that of amorphous Mo_3VO_x (Fig. S1), which possess a layered-structure in the *c*- direction with an interval layer distance of 4.01 Å. The arrangement of the *a-b* plane of amorphous Mo_3VO_x is a network of pentagonal units.[23] The results of XRD suggested that the arrangement of niobium oxide in the *a-b* plane is also a deformed orthorhombic structure as shown Fig. 2b. In the case of the NbO-ANO sample, the interval layer distance of Nb-O-Nb was 3.92 Å, calculated from the diffraction peak. This distance is smaller than
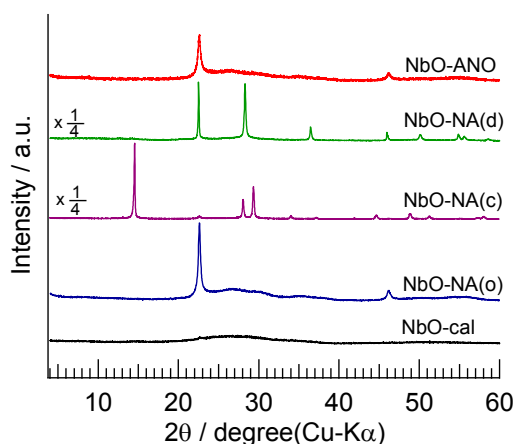
that of Mo-O-Mo, due to Nb octahedra which trends to be more symmetric than Mo. High-resolution transmission electron microscopy (HRTEM) images and selected area electron diffraction of NbO-ANO were collected to confirm the crystal structure (Fig. 2a). The layer distance in the *c*-direction was estimated to be 3.91 Å from HRTEM images, which is in good agreement with the results obtained from the XRD pattern of that catalyst. Leite et al. reported the synthesis of pseudohexagonal niobium oxide nanorods by hydrothermal treatment (140 °C) of a niobium peroxo complex precursor formed by ammonium niobium oxalate ($NH_4[NbO(C_2O_4)_2(H_2O)_2] \cdot nH_2O$) and hydrogen peroxide[7]. It is thought that these different phases of the layered-type and pseudohexagonal niobium oxides were formed due to the different niobium precursors and hydrothermal conditions.

Niobic acid, which is often used as a solid acid, was also subjected to hydrothermal synthesis. Crystalline niobium oxides possessing a pseudohexagonal phase (NbO-NA(d)) and pyrochlore phase (NbO-NA(c)) were synthesized by adjusting the amount of niobic acid in the precursor solution, and their diffraction patterns are shown in Fig. 1. Fig. S2 shows the effects of the amount of niobic acid on the XRD patterns of niobium oxides obtained before calcination. The sample obtained from 0.25 mmol Nb_2O_5 in 40 mL deionized water (NbO-NA(d)) gave diffraction peaks at $2\theta = 22.5$, 28.3, 36.5, 46.0, 50.1, 54.9°. This pattern was in agreement with the pseudohexagonal structure called $TT-Nb_2O_5$ phase (JCPDS 28-0317, lattice constants: c= 3.94 Å and a= 3.64 Å). The structure of $TT-Nb_2O_5$ is shown in Fig. 2c. The *a-b* plane is comprised of edge-shared NbO_6 and NbO_7 units. These are linked by corner-sharing polyhedra along the *c*-axis to form the three-dimensional structure.[33–35] The XRD patterns for niobium oxide obtained from 4 mmol Nb_2O_5 in 40 mL deionized water (NbO-NA(c)) gave diffraction peaks at $2\theta = 14.5$, 28.0, 29.2, 33.9, 37.0, 41.8, 44.5, 48.7, 51.1, 57.1, 57.9° (Fd-3m(227), JCPDS 61-0608), which are ascribable to a pyrochlore type crystalline structure (Fig. 2d). The pyrochlore structure is comprised of corner-shared NbO_6. There are a few reports for pyrochlore $H_4Nb_2O_7$. Wu et al. reported photocatalytic activity over pyrochlore $H_4Nb_2O_7$ obtained by a hydrothermal method,[2] and Nalbandyan et al. described a method for synthesis by a solid state reaction in the JCPDS data base. In the case of ammonium niobium oxalate precursor, regardless of the concentration in the range from 0.0125 to 0.25 mol L⁻¹, the XRD patterns of the niobium oxide samples gave the same peaks at $2\theta =$

Fig. 1 XRD patterns for various niobium oxides after heat treatment.

Table 1 Results of characterization of various niobium oxides obtained by a hydrothermal method

| Catalyst	Synthesis method	Calcination temp./ °C	Crystallinity	d(001)	Morphology (particle size /nm)	BET surface area / m² g⁻¹	*t*-plot / m² g⁻¹	Mesopore volume[a] / cm³ g⁻¹
NbO-ANO	Hydrothermal	400	Deformed orthorombic	3.922	Rod(10×50~100)	193	202	0.563
NbO-NA(d)	Hydrothermal	400	Pseudohexagonal($TT-Nb_2O_5$)	3.938	Rod(200×2000)	47	48	0.228
NbO-NA(c)	Hydrothermal	300	Pyrochlore	-	Sphere(50~250)	38	38	0.035
NbO-NA(o)	Hydrothermal	400	Deformed orthorhombic	3.928	Rod(10×30~50)	100	107	0.131
NbO-cal	Calcination	400	Amorphous	-	Sphere(50~250)	27	27	0.002
NbO-ANO	Hydrothermal	500	Deformed orthorhombic	3.921	n.d.	113	115	0.071
NbO-ANO	Hydrothermal	550	Orthorhombic($T-Nb_2O_5$)	3.935	n.d.	66	67	0.010
NbO-ANO	Hydrothermal	700	Orthorhombic($T-Nb_2O_5$)	3.933	n.d.	21	21	0.003

[a] Calculated by the BJH method.
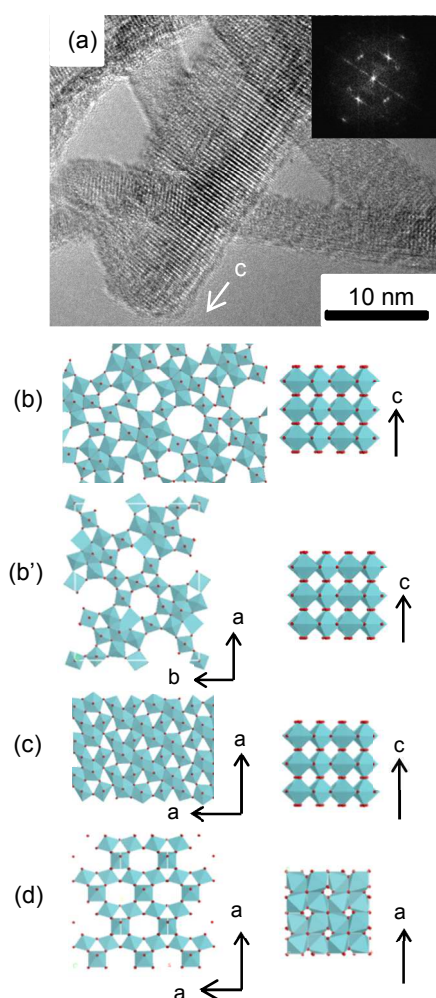
Fig. 2 (a) HRTEM image and electron diffraction of NbO-ANO, (b) proposed structure model of NbO-ANO (deformed orthorhombic), and (b') crystalline models of orthorhombic, (c) pseudohexagonal (TT- Nb_2O_5) and orthorhombic (T-Nb_2O_5) niobium oxides, and (d) pyrochlore niobium oxide. (Blue octahedron: Nb-O octahedron, red dot: oxygen)

22.7° and 46.2° (Fig. S3).

Niobium oxide was also synthesized under hydrothermal conditions from a mixture of niobic acid and oxalic acid. Oxalic acid was added to a niobic acid (2 mmol)-dispersed solution. By the addition of more than 0.125 mol L^{-1} oxalic acid, niobic acid was completely dissolved. Fig. S4 shows the effects of the ratio of oxalic acid and niobium acid on the XRD pattern of niobium oxide. In the case of only niobic acid, the diffraction pattern was a mixture of layered, pseudohexagonal and pyrochlore structures, and the peaks based on the pyrochlore structure were decreased by calcination at 400 ˚C, while the peaks based on the pseudhexagonal phase remained as described later. The peaks based on the pyrochlore and pseudohexagonal structures were decreased by the addition of oxalic acid, and peaks of the pyrochlore and pseudohexagonal structures were not observed by the addition of 0.25 mol L^{-1} oxalic acid. This sample was denoted as NbO-NA(o). The XRD pattern of the NbO-NA(o) sample showed peaks at 2θ = 22.7° and 46.2° as in the case of NbO-ANO. For niobium oxide synthesis by a hydrothermal process,

it is considered that niobium oxide is formed through a dissolution–crystallization mechanism and rearrangement of niobium polyhedra occurs. In the presence of oxalic acid, Nb forms pentagonal bipyramidal units with an oxalate ligand in the precursor solution, and the pentagonal $\{Nb_6O_{21}\}$ units would be formed under hydrothermal conditions. The pentagonal units play an important role in the formation of a new crystalline structure under hydrothermal condition.

Fig. S5 shows STEM images of the obtained niobium oxides synthesized under hydrothermal conditions, and their morphologies are summarized in Table 1. NbO-ANO consists of one-dimensional nanorods with diameters of ca. 10 nm and lengths of 50-100 nm. The nanorods suggest growth along the [001] direction. NbO-NA(o) was also nanorods with diameters of ca. 10 nm and lengths of 30-50 nm. NbO-NA(d) was relatively large rods with diameters of ca. 200 nm and lengths of 2 μm. NbO-NA(c) and NbO-cal consist of spherical particles with diameters of 50-250 nm.

The samples were heat-treated at different temperatures under air in order to examine their thermal stability. Fig. 3 shows the effect of calcination temperature on XRD patterns of NbO-ANO and NbO-NA(c). The XRD patterns of the as-synthesized NbO-ANO showed tense and sharp peaks at 2θ = 22.7° and 46.2° as described above. The structure of layered niobium oxide was maintained after 500 ˚C treatment. When NbO-ANO was calcined at 550 and 700 ˚C, the peaks at 22.7° shifted to lower angles and diffraction peaks based on orthorhombic niobium oxide (T- Nb_2O_5, Pbam (55), JCPDS 30-0837) appeared. The orthorhombic (T- Nb_2O_5) and pseudohexagonal (TT-Nb_2O_5) phases are difficult to distinguish in terms of structure. The T phase is thought to be simply a more ordered structure of the TT phase (Fig. 2c). [33–35] The pyrochlore sample was not stable for heat treatment. The positions of the diffraction peaks of samples heat-treated at 200 and 300 °C for 4 h did not shift, but intensities of the peaks decreased with increase in the calcination temperature. The diffraction pattern of pyrochlore niobium oxide calcined at a temperature higher than 400 °C was hexagonal phase, revealing a phase transition. And the monoclinic phase was observed in the sample calcined at 800 °C. In order to evaluate the characteristic of pyrochlore structure, NbO-(c) was treated at 300 °C.
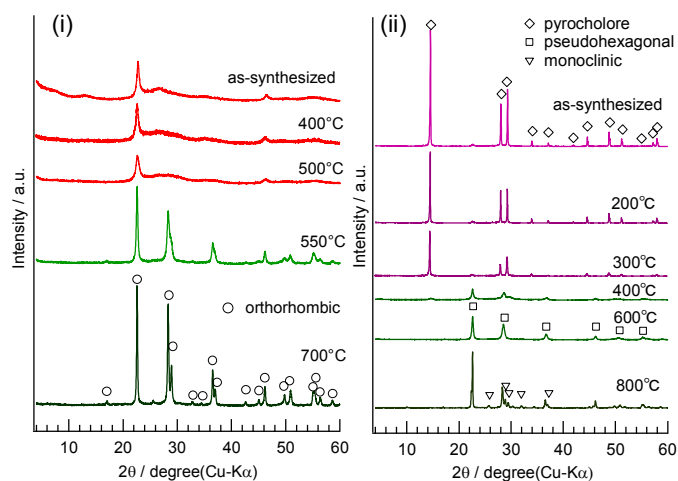
Raman spectroscopy was performed to confirm the

Fig. 3 Effects of the calcination temperature on the XRD patterns of (i) NbO-ANO and (ii) NbO-NA(c).
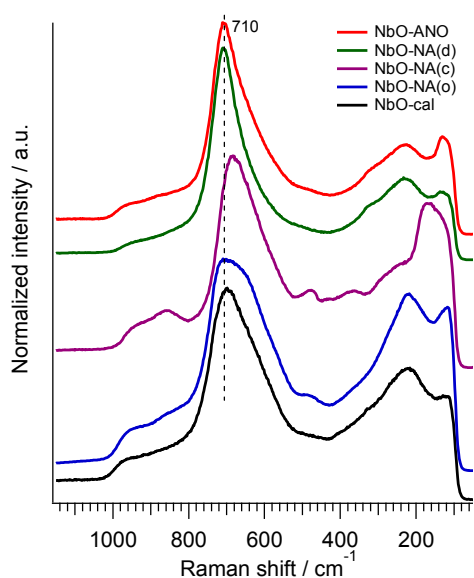
Fig. 4 Raman spectra of various niobium oxides synthesized by a hydrothermal method and niobic acid.

niobium oxide structure of the NbO-ANO catalyst. The Raman band in the 500- 800 cm^{-1} is assigned to symmetric stretching modes of slightly distorted NbO_6 octahedra, and associated bending modes of Nb-O-Nb linkages appear in the low wavenumber region around 200 cm^{-1}.[13, 14] In the case of pseudohexagonal (TT- phase) Nb_2O_5, the Raman band of symmetric stretching modes of NbO_6 octahedra is observed in around 700 cm^{-1}. The weak broad Raman band around 900 cm^{-1} is assigned to the symmetric stretching mode of Nb=O surface sites. Fig. 4 shows Raman spectra of obtained niobium oxides obtained after calcination. The Raman band of the pyrochlore NbO-NA(c), corner-shared structure of NbO_6 octahedra, showed a characteristic band based on the symmetric stretching modes (690 cm^{-1}) and the bending modes of Nb-O-Nb linkage (260, 365, 475 cm^{-1}). The Raman band at 170 cm^{-1} was assigned to translational modes of Nb, and the Raman band at 860, 940 cm^{-1} was assigned to the symmetric stretching mode of terminal Nb-O for the pyrochlore NbO-(c).[36] The Raman band at 710 cm^{-1} of the pseudohexagonal NbO-NA(d), which possesses NbO_6 octahedra and NbO_7 in its structure, is assigned to the symmetric stretching mode of polyhedra. The Raman band at 230, 970 cm^{-1} were assigned to the bending modes of Nb-O-Nb linkage and the symmetric stretching mode of Nb=O, respectively. The Raman band of NbO-ANO was almost the same as that of NbO-NA(d), indicating that NbO-ANO also consists of NbO_6 and NbO_7. For the NbO-cal and NbO-NA(o) samples, the band of the symmetric stretching mode of polyhedra shifted to 690 cm^{-1}. For the NbO-NA(o) sample, the band of the symmetric stretching mode of polyhedra

was broadened compared to that of the NbO-NA(d) sample, indicating that these samples contain distorted NbO_6 octahedra, NbO_7 pentagonal bipyramids and NbO_8 hexagonal bipyramids. [13]

The XRD pattern and Raman spectra of NbO-ANO indicated that NbO-ANO is a layered-structure composed of NbO_6 octahedra and NbO_7 pentagonal bipyramids interconnected in the *a-b* plane. This structure can be regarded as a niobium bronze structure based on pentagonal $\{Nb_6O_{21}\}$ building units. Lundberg et al. reported orthorhombic $Cs_x(Nb,W)_5O_{14}$[32] that possesses a tungsten or niobium bronze structure based on the pentagonal unit. This $Cs_x(Nb,W)_5O_{14}$ was synthesized by solid state reaction at a high temperature, so that a small surface area (3 m^2 g^{-1}) is inevitable and it is difficult to remove the cesium cations in the heptagonal channnel.[29] We have reported that the molybdenum bronze based on the pentagonal $\{Mo_6O_{21}\}$ unit of orthorhombic Mo_3VO_x obtained by a hydrothermal method. Ammonium cations derived from the precursor are located in the heptagonal channel and they can be removed as ammonia by calcination. After calcination, the heptagonal channel acts as a micropore. [23] Therefore, the presence of micropores confirms the formation of a bronze structure as orthorhombic phase (Fig. 2b'). In order to investigate the microporosity, N_2 adsorption of NbO-ANO, NbO-Nb(d), NbO-NA(c), NbO-NA(o) and NbO-cal was examined (Fig. S6), and calculated data are summarized in Table 1. The orthorhombic Mo_3VO_x showed N_2 adsorption at a relative pressure P/P$_0$ lower than 1.0×10^{-5}, revealing microporosity. The NbO-ANO sample also showed N_2 adsorption at low pressure (1.0×10^{-6}), suggesting formation of micropores like heptagonal channels. In addition, the difference in surface area between the BET method and the *t*-method indicates the existence of micropores. After the adsorption at 1.0×10^{-6}, the amount of adsorbed nitrogen gradually increased with nitrogen pressure for NbO-ANO, suggesting that the micropores formed within NbO-ANO are partially non-uniform. NbO-NA(o) and NbO-NA(d) also adsorbed N_2 at relatively low pressure, but the adsorption volume increased gradually, implying that the size of micropores was not ordered. NbO-NA(c) and NbO-cal did not show

Table 2 Alkylation over various niobium oxides

Catalyst	Calcination temp. /^{o}C	Acid amounts[a]		Conv. (benzyl alcohol)/ % (yield (benzyl anisole)/ %)		F. r.[b] /mmol h^{-1} m^{-2}
		mmol g^{-1}	µmol m^{-2}	Condition I[b]	Condition II[c]	
NbO-ANO	400	0.152	0.788	100 (93.9)	51.7 (36.4)	0.094
NbO-NA(d)	400	0.025	0.532	82.8 (77.6)	5.4 (2.7)	0.029
NbO-NA(c)	300	1.362	-	0.0 (0.0)	0.0 (0.0)	0.000
NbO-NA(o)	400	0.078	0.729	100 (91.6)	20.7 (11.6)	0.054
NbO-cal	400	0.008	0.296	12.4 (8.6)	2.1 (1.3)	0.024
NbO-ANO	500	0.028	0.248	100 (96.3)	43.6 (26.2)	0.116
NbO-ANO	550	0.003	0.045	31.2 (29.1)	14.9 (9.7)	0.073
NbO-ANO	700	0.000	0.000	4.5 (0.8)	0.0 (0.0)	0.000
NbO-ANO(K$^+$)	400	0.038	0.208	5.6 (0.7)	0.0 (0.0)	0.000
NbO-ANO(NH$_4^+$)	400	0.168	0.840	100 (93.2)	43.6 (28.2)	0.071

[a] Acid amounts were calculated by NH$_3$-TPD and BET surface area, [b] formation rate of benzyl anisole per BET surface area for condition II, [c] reaction condition I: benzyl alcohol (1.0 mmol), anisole (50 mmol), catalyst (0.1 g), 100 ^{o}C , 30 min, [d] reaction condition II: benzyl alcohol (10 mmol), anisole (100 mmol), catalyst (0.1 g), 100 ^{o}C , 120 min.
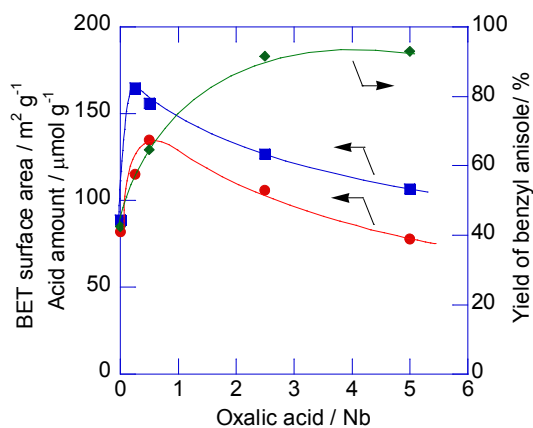
Fig. 5 Effects of the ratio of oxalic acid and niobium oxide in the precursor solution on the BET surface area (■), acid amount calculated by NH_3-TPD (●) and alkylation result (◆) for the obtained sample. (Reaction condition was condition I in Table 2.)

N_2 adsorption at a low pressure.

Results of XRD, Raman and adsorption analyses suggested that the *a-b* plane of NbO-ANO is a deformed orthorhombic structure as illustrated in Fig. 2b. The deformed orthorhombic structure in the *a-b* plane perpendicular to the *c*-axis is an interconnection of crystal structure motifs such as $\{Nb_6O_{21}\}$ pentagonal units and micropore channels but without any long-range order. In order to confirm the structure, TPD-MS, TG and XPS were carried out (Fig. S7, S8). From these analyses, the formula of as-synthesized NbO-ANO can be expressed as $H_{19.9}(NH_4)_{4.1}Nb_{40}O_{112}\cdot 3.6H_2O$, calculated on the basis of a lattice unit of the orthorhombic phase. The elemental composition is expressed as $A^I_4M^{V/VI}_{40}O_{112}\cdot nH_2O$ (A: cation, M: metal) for the orthorhombic structure. The ratio of ammonia cation to metal was matched from a structural point of view. This result indicated that NH_3 is located in the heptagonal channel.

NH_4^+ formed by NbO_6 octahedra (NH_4-ONb) in the heptagonal channel can be released by calcination, and Brönsted acid sites (HO-Nb) will be produced. Thus, the solid acid catalytic activity was examined about the relationship between the structure and catalytic activity. Results for the Friedel-Crafts alkylation reactions of anisole with benzyl alcohol over various niobium oxides are presented in Table 2 and Fig. S9. Several catalysts showed 100 % conversion under the condition I, therefore catalytic test were also conducted under the condition II in order to compare the catalytic activity. Acid amounts of niobium oxides were measured by NH_3-TPD (Fig. S10 and Table 2). The products were benzyl anisole and dibenzyl ether. Carbon balance was always more than 97% in all experiments. The NbO-ANO (deformed orthorhombic) catalyst had the highest activity, with 100% conversion of benzyl alcohol and with 94% yield (benzyl anisole) under the condition I. Catalyst reuse experiment was tested under the condition II for three runs(Fig. S11). The collected catalyst was repeatedly rinsed with acetone and dried in the oven at 80 ºC. No significant decrease in benzyl alcohol conversion and benzyl anisole yield were observed

after three reuses of the catalyst. The conversion of benzyl alcohol decreased with increase in the heat treatment temperature, and the NbO-ANO sample calcined at 550 ºC showed 31% conversion with 29% yield, NbO-ANO calcined at 700 ºC (orthorhombic, T-Nb_2O_5) showed no catalytic activity. NbO-NA(d) (pseudohexagonal) samples (83% conversion, 78% yield) and NbO-cal (amorphous) samples (12% conversion, 9% yield) showed less activity.

NbO-NA(c) (pyrochlore) showed no catalytic activity as a solid acid, even though it adsorbed many NH_3 molecules as revealed by NH_3-TPD. The amount of absorbed NH_3 was 1.36 mmol g^{-1} when NH_3 was adsorbed at 150 ºC, and this value corresponded to $(NH_4)_{0.36}Nb_2O_5\cdot nH_2O$. The adsorbed NH_3 would be located inside the hexagonal channel like other pyrochlore type $A_2Nb_2O_7$,[37–39] and this site potentially acts as a solid acid site, but the hexagonal channel is too small for an organic substrate to access.

The NbO-NA(o) samples showed less activity than that of NbO-ANO under the condition II (Table 2). Fig. 5 shows the results of characterization and alkylation reaction for niobium oxide obtained from the mixture of niobic acid and oxalic acid. By the addition of oxalic acid to niobic acid, the BET surface area and acid amount increased, and with an increase in the concentration of oxalic acid, the BET surface area and acid amount gradually decreased. On the other hand, the yield of benzyl anisole increased with increase in the oxalic acid concentration in the precursor solution. Although NbO-NA(o) showed an XRD pattern similar to that of NbO-ANO, the catalytic activities were different under the condition II. From the Raman spectra of NbO-NA(o), the band of the symmetric stretching mode of niobium polyhedra was broad (Fig. 4) and the N_2 adsorption at low pressure indicated that micropores based on the heptagonal channel were not formed orderly. In the case of orthorhombic Mo_3VO_x, the cation in the precursor solution acts as a stabilizer and a structure-directing agent under hydrothermal conditions.[40] For niobium oxide, it is considered that the ammonium cation has an important role in the formation of a uniformed crystalline structure and micropores based on the heptagonal channel. These results also suggested that a stronger Brönsted acid site was formed around the open mouth of the heptagonal channel after desorption of ammonia.

A comparison of the formation rates of benzyl anisole per surface area showed that the order of catalytic activity was NbO-ANO (deformed orthorhombic)> NbO-NA(o)> NbO-NA(d) (TT-Nb_2O_5), NbO-cal (amorphous)>> NbO-ANO(T-Nb_2O_5), NbO-NA(c) (pyrochlore). It is difficult to relate the acid amount to alkylation activity because the acid amount calculated by NH_3-TPD includes both Lewis acid and Brönsted acid sites. It is known that the activity of alkylation of anisole and benzyl alcohol over niobic acid can be promoted on Brönsted acid sites.[16–22] To demonstrate the effect of Brönsted acid site, ion exchange treatments were conducted. After K^+-exchange treatment (NbO-ANO(K^+)), 85% of NH_4^+ in the niobium oxide was ion-exchanged by K^+ as confirmed by TPD measurement (Fig. S12). IR spectra also confirmed that NH_4^+ existed in the NbO-ANO precursor and NH_4^+ was removed by

the ion exchange treatment. In addition, after NH_4^+-exchange treatment of NbO-ANO(K^+), the amount of NH_4^+ in NbO-ANO(NH_4^+) was 81% of NbO-ANO. NbO-ANO (K^+) showed no activity for alkylation reaction of benzyl alcohol. On the other hand, NbO-ANO(NH_4^+) showed activity similar to that of NbO-ANO (Table 2). These results suggested that the NbO-ANO possess the ion-exchange capacity. The ion exchange treatment by K^+ deactivated the Brönsted acid sites but these sites were recovered by the further ion-exchange by NH_4^+ and the calcination.

NbO-ANO ($H_{19.9}(NH_4)_{4.1}Nb_{40}O_{112}\cdot3.8H_2O$) desorbed NH_3 and water during calcination at 400 °C without changing its structure. A Brönsted acid site would be formed around the open mouth of the heptagonal channel after desorption of ammonia. This acid site of NbO-ANO can explain the solid acid activity for crystalline niobium oxide. A more crystalline niobium oxide must to be prepared for its exact structure analysis. However, layered-structure niobium oxide formed by NbO_6 octahedra and NbO_7 pentagonal bipyramids, possessing a crystalline structure such as an orthorhombic structure, would form exceptional acid sites.

Conclusions

Crystalline niobium oxides (deformed orthorhombic, pseudohexagonal (TT-Nb_2O_5), orthorhombic (T-Nb_2O_5) and pyrochlore niobium oxides) were synthesized by a hydrothermal process. The NbO-ANO sample obtained from ammonium niobium oxalate showed a layered-type structure, in which NbO_6 octahedra were corner-sharing in the c-direction. Raman spectra indicated that the layered niobium consisted of NbO_6 octahedra and NbO_7 in its structure. Adsorption results showed the presence of micropore channels, indicating the formation of a high-dimensional structure in the a-b plane. From these results, we concluded that the structure of NbO-ANO was deformed orthorhombic phase. As-synthesized NbO-ANO was expressed as $H_{19.9}(NH_4)_{4.1}Nb_{40}O_{112}\cdot3.8H_2O$, and NH_3 and water were desorbed by calcination at 400 °C, forming Brönsted acid without changing its structure. This material showed the high catalytic activity as a solid acid. The layered-structure niobium oxide composed of NbO_6 octahedra and $\{Nb_6O_{21}\}$ pentagonal units forms exceptional Brönsted acid around the open mouth of the heptagonal channel.

Acknowledgements

Notes and references

^{a} Catalysis Research Center, Hokkaido University, N-21, W-10, Sapporo 001-0021, Japan. E-mail: murayama@cat.hokudai.ac.jp(Murayama), ueda@cat.hokudai.ac.jp(Ueda); Fax: +81 11 706 9163; Tel: +81 11 706 9164.

1. A. Llordés, G. Garcia, J. Gazquez, and D. J. Milliron, *Nature*, 2013, **500**, 323–326.
2. J. Wu, J. Li, X. Lü, L. Zhang, J. Yao, F. Zhang, F. Huang, and F. Xu, *J. Mater. Chem.*, 2010, **20**, 1942–1946.
3. K. Tanabe and S. Okazaki, *Appl. Catal. A, Gen.*, 1995, 133, 191–218.
4. K. Nakajima, Y. Baba, R. Noma, M. Kitano, J. N. Kondo, S. Hayashi, and M. Hara, *J. Am. Chem. Soc.*, 2011, **133**, 4224–4227.
5. C. Feldmann and H.-O. Jungk, *Angew. Chemie Int. Ed.*, 2001, **40**, 359–362.
6. N. Uekawa, T. Kudo, F. Mori, Y. J. Wu, and K. Kakegawa, *J. Colloid Interface Sci.*, 2003, **264**, 378–384.
7. E. R. Leite, C. Vila, J. Bettini, and E. Longo, *J. Phys. Chem. B*, 2006, **110**, 18088–18090.
8. Y. Zhou, Z. Qiu, M. Lü, A. Zhang, and Q. Ma, *J. Lumin.*, 2008, **128**, 1369–1372.
9. M. Mozetič, U. Cvelbar, M. K. Sunkara, and S. Vaddiraju, *Adv. Mater.*, 2005, **17**, 2138–2142.
10. W. Hu, Z. Liu, G. Nie, Y. Mi, Y. Zhao, and K. Yao, *Mater. Chem. Phys.*, 2009, **113**, 511–514.
11. N. Pinna, M. Antonietti, and M. Niederberger, *Colloids Surfaces A Physicochem. Eng. Asp.*, 2004, **250**, 211–213.
12. W. Fan, Q. Zhang, W. Deng, and Y. Wang, *Chem. Mater.*, 2013, **25**, 3277–3287.
13. J. M. Jehng and I. E. Wachs, *Chem. Mater.*, 1991, 100–107.
14. R. Brayner and F. Bozon-Verduraz, *Phys. Chem. Chem. Phys.*, 2003, **5**, 1457–1466.
15. V. Lebarbier, M. Houalla, and T. Onfroy, *Catal. Today*, 2012, **192**, 123–129.
16. Y. Rao, M. Trudeau, and D. Antonelli, *J. Am. Chem. Soc.*, 2006, **128**, 13996–13997.
17. M. Delacruz, J. Dasilva, and E. Lachter, *Catal. Today*, 2006, **118**, 379–384.
18. R. M. West, Drew J. Braden, and J. A. Dumesic, *J. Catal.*, 2009, **262**, 134–143.
19. A. Takagaki, M. Sugisawa, D. Lu, J. N. Kondo, M. Hara, K. Domen, and S. Hayashi, *J. Am. Chem. Soc.*, 2003, **125**, 5479–5485.
20. C. Tagusagawa, A. Takagaki, S. Hayashi, and K. Domen, *J. Am. Chem. Soc.*, 2008, **130**, 7230–7231.
21. K. Yamashita, M. Hirano, K. Okumura, and M. Niwa, *Catal. Today*, 2006, **118**, 385–391.
22. T. Shishido, T. Kitano, K. Teramura, and T. Tanaka, *Catal. Letters*, 2009, **129**, 383–386.
23. T. Konya, T. Katou, T. Murayama, S. Ishikawa, M. Sadakane, D. Buttrey, and W. Ueda, *Catal. Sci. Technol.*, 2013, **3**, 380–387.
24. S. Ishikawa, X. Yi, T. Murayama, and W. Ueda, *Catal. Today*, 2014, 8–13.
25. S. Ishikawa, X. Yi, T. Murayama, and W. Ueda, *Appl. Catal. A Gen.*, 2014, **474**, 10–17.
26. M. Sadakane, N. Watanabe, T. Katou, Y. Nodasaka, and W. Ueda, *Angew. Chem. Int. Ed. Engl.*, 2007, **46**, 1493–1496.
27. M. Sadakane, K. Kodato, T. Kuranishi, Y. Nodasaka, K. Sugawara, N. Sakaguchi, T. Nagai, Y. Matsui, and W. Ueda, *Angew. Chem. Int. Ed. Engl.*, 2008, **47**, 2493–2496.
28. T. Murayama, N. Kuramata, S. Takatama, K. Nakatani, S. Izumi, X. Yi, and W. Ueda, *Catal. Today*, 2012, **185**, 224–229.

29. K. Omata, S. Izumi, T. Murayama, and W. Ueda, *Catal. Today*, 2013, **201**, 7–11.

30. K. Omata, K. Matsumoto, T. Murayama, and W. Ueda, *Chem. Lett.*, 2014, **43**, 435–437.

31. N. Galešić, N. Brničević, B. Matković, M. Herceg, B. Zelenko, M. Šljukić, B. Prelesnik, and R. Herak, *J. Less Common Met.*, 1977, **51**, 259–270.

32. M. Lundberg and M. Sundberg, *Ultramicroscopy*, 1993, **52**, 429–435.

33. K. Kato and S. Tamura, *Acta Crystallogr. Sect. B*, 1975, **31**, 673–677.

34. H. Schäfer, R. Gruehn, and F. Schulte, *Angew. Chemie Int. Ed. English*, 1966, **5**, 40–52.

35. Y. Kobayashi, H. Hata, M. Salama, and T. E. Mallouk, *NANO Lett.*, 2007, **7**, 2142–2145.

36. M. Mączka, a V Knyazev, A. Majchrowski, J. Hanuza, and S. Kojima, *J. Phys. Condens. Matter*, 2012, **24**, 195902.

37. Z. Zou, J. Ye, and H. Arakawa, *Chem. Mater.*, 2001, **13**, 1765–1769.

38. Z. Zou, J. Ye, and H. Arakawa, *J. Phys. Chem. C*, 2002, **106**, 517–520.

39. L. Zhang, H. Fu, C. Zhang, and Y. Zhu, *J. Phys. Chem. C*, 2008, **112**, 3126–3133.

40. S. Ishikawa, T. Murayama, S. Ohmura, M. Sadakane, and W. Ueda, *Chem. Mater.*, 2013, **25**, 2211–2219.

Catalysis Science & Technology Accepted Manuscript

Graphical abstract

Synthesized niobium by hydrothermal method